Optical properties of cluster-assembled nanoporous gold films

F. Bisio,[1,2,*] M. Palombo,[2] M. Prato,[3] O. Cavalleri,[2] E. Barborini,[4] S. Vinati,[4] M. Franchi,[4] L. Mattera,[2] and M. Canepa[2]
[1]*CNR–INFM LAMIA, C.so Perrone 24, 16152 Genova, Italy*
[2]*CNISM, Sede Consorziata di Genova and Dipartimento di Fisica, Università di Genova, via Dodecaneso 33, 16146 Genova, Italy*
[3]*Istituto Nazionale di Fisica Nucleare–Sezione di Genova, Via Dodecaneso 33, 16146 Genova, Italy*
[4]*Tethis Srl, Via Franco Russoli 3, 20143 Milan, Italy*
(Received 20 August 2009; revised manuscript received 9 October 2009; published 30 November 2009)

We report a spectroscopic ellipsometry investigation of the electronic and morphological properties of cluster-assembled nanoporous metallic gold films deposited from a low-energy supersonic cluster beam. We modeled the optical response of the medium by explicitly introducing a variable degree of porosity in the film and finite-size effects due to the cluster nanometeric size. We deduced the characteristic size of the individual clusters within the nanoporous structure and their depth-resolved arrangement. Comparison with independent data available in the literature yielded extremely good quantitative agreement with the results extracted from our model, in terms of the degree of porosity of the films and of their surface roughness. The cluster-size distribution in the films obtained by the optical model matched extremely well the one obtained by atomic-force microscopy on isolated clusters. This demonstrates that, though the clusters are in contact with one another in the porous film, they retain their crystallographic individuality when assembled in three-dimensional structures.

DOI: 10.1103/PhysRevB.80.205428 PACS number(s): 78.67.Bf

I. INTRODUCTION

One of the most remarkable differences that porous materials exhibit with respect to their bulk counterparts is the availability of tremendous enhancements of free-surface areas per unit volume. This property concurs to make porous materials extremely appealing as high-efficiency catalysts and molecular sensors, and has accordingly fuelled huge research efforts in this direction in the past years. Porous materials exhibiting typical pore size in the few nanometer range (nanoporous) provide additional motivation for interest as selective molecular detectors since the pore dimension is directly compatible with the typical size of macromolecules.[1,2]

Among nanoporous materials, metals are receiving particular attention due to the possibility of exploiting the influence of finite-size effects on their optical response (plasmon resonances) for ultrasensitive optical detection.[3,4] Such type of application offers the relevant advantage of directly exploiting the several inherent advantages of optical techniques. Optical probes are in fact nondestructive, especially when molecules are involved,[5] are fast and straightforward to employ and, not least, can probe the material response within a volume limited only by the radiation skin depth.

Fully exploiting the potential of optical techniques in the analysis of nanoporous materials, requires going beyond a merely qualitative analysis of the spectra and developing reliable models of the optical response of the material that keep its nanoscale structure into account.[6–9] Successfully modeling the system's response yields in turn extremely valuable information about the parameters of the nanoporous structure such as void fraction and mean characteristic dimension of the metallic frame, that are typically fundamental in determining its overall properties.

In this paper we report a variable-angle spectroscopic ellipsometric investigation of the morphological and electronic properties of thin nanoporous cluster-assembled Au films deposited from a supersonic cluster beam. Cluster-assembled materials are a class of materials that have stimulated great interest from the scientific and applicative point of view, due to their application as sensors,[10] biocompatible supports,[11] and in general for the versatile fabrication of complex three-dimensional nanostructures endowed with novel interesting properties.[12] Gold is at the hearth of a widespread interest in the field of nanoporous structure for (bio)molecule sensing and for plasmonics applications. In this work, we modeled the optical response of the cluster-assembled medium by both applying a cluster-size-dependent correction to account for the granular nature of the films[6,7,13] and explicitly introducing a depth-dependent degree of porosity in the medium. This allowed us to deduce the effective characteristic size of the individual building blocks of the nanoporous structure and their arrangement in a porous films. Comparison with data obtained by atomic-force microscopy and with theoretical simulations available in the literature yielded a good quantitative agreement with our results, in terms of the degree of porosity of the Au structures and of their surface roughness. Matching the cluster-size distribution obtained by atomic-force microscopy with the effective-mean cluster size extracted by optical modeling yielded a good agreement between the two methods. This provided a direct confirmation of the success of the optical modeling, and suggests that the low-energy assembled clusters maintain, from a crystallographic point of view, their individuality when randomly stacked in a three-dimensional structure.

II. EXPERIMENT

A. Preparation of nanoporous Au samples

Nanostructured Au films with variable thickness in the tens of nanometer range deposited onto 15×15 mm^2 silicon

 ©2009 The American Physical Society

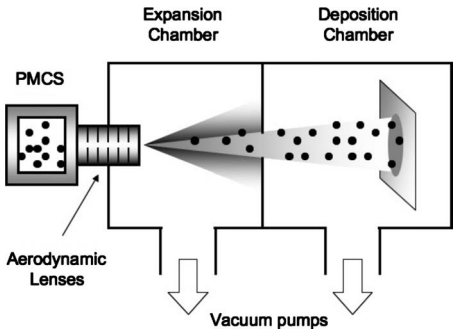

FIG. 1. Schematic of the SCBD experimental apparatus employed for nanoporous Au film deposition.

wafers were fabricated by the Tethis Srl company. The films were produced by supersonic cluster beam deposition (SCBD), using an apparatus equipped with a pulsed microplasma cluster source (PMCS), as schematically shown in Fig. 1. The principle of operation of a PMCS, described in detail in Refs. 14 and 15, is based on the ablation of a rod-shaped target by an inert gas plasma pulse ignited by a pulsed electric discharge: the ablated atoms thermalize into the inert gas and reaggregate to form clusters. The gas-cluster mixture undergoes supersonic expansion driven by pressure difference between the source and the expansion chamber. A group of aerodynamic lenses[16] collects the gas-cluster stream from PMCS nozzle and forces the nanoparticles to concentrate close to the beam axis, increasing the beam collimation (divergence less than 20 mrad) and the in-axis intensity. Aerodynamic lenses also act as a mass filter, removing the coarse tail of the particle size distribution. The beam collimation allows the separation of the deposition chamber from the expansion chamber, with a differential vacuum approach, in order to reach ultraclean conditions in the deposition chamber, where the growth of cluster-assembled nanostructured films takes place at room temperature. The kinetic energy of about a few tenths of eV per atom, characterizing clusters in supersonic argon beams, promotes a good adhesion of the resulting cluster-assembled film.[17,18] The films were deposited at room temperature, where low particle mobility dominates the growth dynamics.[19,20] The typically observed morphological features of cluster-assembled films can be ascribable to ballistic regime growth. Nanoscale porosity causing lower density respect to bulk and surface roughness increasing with film thickness are the most relevant features.

Prior to deposition, the wafers were cleaned by 30 min immersion in "piranha" solution [30% H_2O_2 (BDH Analar, purity >30%): 70% concentrated H_2SO_4 (Fluka, purity 95–97 %)] at 80 °C, 3 min in HF (Fluka, purity >48%), 30 min again in piranha solution at 80 °C. Each step was followed by careful rinsing in Milli-Q water. This cleaning procedure assures a good hydrophilic substrate, characterized by extremely uniform thickness of the native oxide layer.[21] During deposition, a shadow mask was applied in front of the substrate in order to deposit the clusters on half of the silicon surface only, thereby leaving part of the wafer uncovered with the purpose of independently assessing its morphological and optical quality.

Four sets of samples, characterized by different cluster-assembled film thickness ranging from submonolayer Au coverage to a few tens of nanometer were prepared in a single deposition run. During the course of the deposition the film thickness was roughly estimated by means of a quartz-crystal monitor (QCM) previously calibrated on sacrificial samples by cross comparison with spectroellipsometric measurements. Though the absolute thickness uncertainty determined by QCM can be on the order of $\pm 10\%$, this method ensures a good estimation of the relative thickness ratios for samples prepared within a single deposition run, whose effective thickness is later assessed with more precision by optical modeling. We will henceforth refer to the above sample sets labeling them as A, B, C, and D. Here A refers to the submonolayer sample, and B–D refer to sample sets of increasing thickness for which a "continuous" film consisting of several stacked cluster layers was formed. Upon quick visual inspection, sample A was not discernible from the dark-gray Si substrate, sample B exhibited a faint yellowish patina with a strong grayish background, while samples C and D gradually lost any gray tone and exhibited dark-yellow, highly reflective surfaces.

B. Atomic-force microscopy

Samples with isolated clusters (set A) were used to evaluate the size distribution of film precursors, by atomic-force microscopy (AFM, Digital Instruments Nanoscope Multimode 3A). For these samples the Au cluster coverage was kept to a minimum (<1%) in order to avoid the possibility of cluster coalescence. Careful substrate preparation before deposition, and reference samples not exposed to the cluster beam, were adopted to favor artifacts elimination (or recognition) in AFM images. In order to rule out the contribution of pathological topologies, statistic of in-plane particle diameters was compared with statistic of particle heights to identify the particle subset characterized by the proper height-diameter relation of spheroidal objects. Final size distribution was obtained limiting the statistic to the heights of this subset, therefore removing also the overestimation due to AFM tip radius. Lognormal distribution, as expected for cluster growth by gas-phase monomer aggregation into PMCS, shows a mean size of 2.7 nm and a maximum well below 2 nm, as reported in Fig. 2 (blue-contoured bars). The fractional volume distribution as a function of the particle diameter, obtained by multiplying the size distribution by the particle volume (under the hypothesis of spherical clusters) and normalizing the distribution to unity, is also reported as the solid orange bars. The fractional volume distribution is peaked in correspondence of a particle diameter $d \approx (6.5 \pm 2)$ nm. In the bottom part of Fig. 2, we report a typical AFM image of sample A (image 1), and of sample D (image 2). In the former, isolated Au clusters are clearly discernible on the substrate, while in the latter, the rough, granular surface characteristic of thick cluster-assembled films is apparent.

C. Spectroscopic ellipsometry spectra

The spectroscopic ellipsometry (SE) characterization of the samples was performed by a J. A. Woollam M-2000S

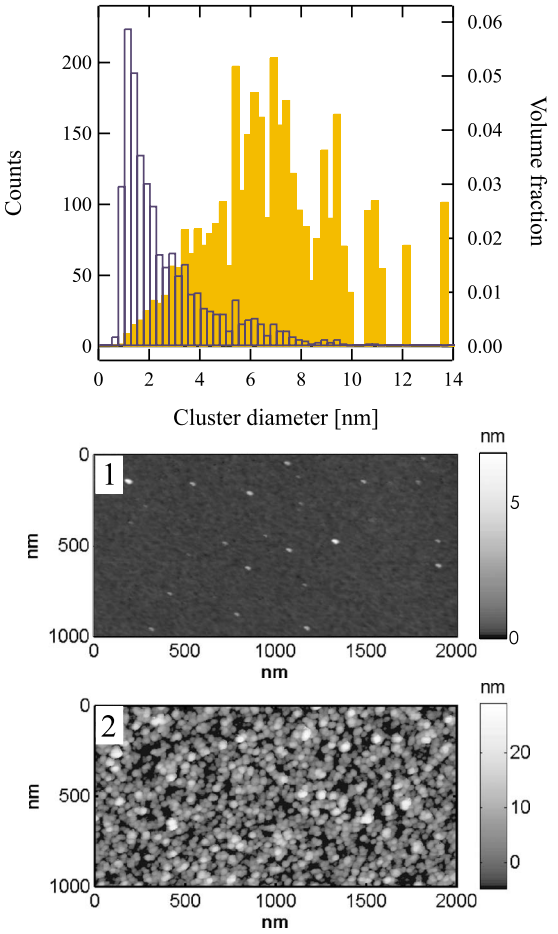

FIG. 2. (Color online) Top: blue-contoured bars: size distribution of Au precursors extracted from the AFM characterization of submonolayer samples. Solid orange bars: fractional volume distribution extracted from the precursor distribution by multiplying it by the cluster volume and normalizing the obtained distribution to unity. See text for details. Bottom: representative AFM images of sample A (image 1) and sample D (image 2).

rotating-compensator spectroscopic ellipsometer, capable of measuring at 225 wavelengths in the 245–725 nm spectral range, at angles of incidence adjustable between 40° and 90°. The principles of ellipsometry are thoroughly described in a number of publications.[22–24] The output of the standard SE measurements is the ratio ρ of the p-polarized and s-polarized complex Fresnel reflection coefficients r_{pp} and r_{ss}, routinely expressed in terms of the two angles Ψ and Δ as

$$\rho = \frac{r_{pp}}{r_{ss}} = \tan \Psi e^{i\Delta}. \quad (1)$$

In order to obtain physical information on the systems under scrutiny, samples are typically modeled as a stack of j layers, each characterized by its complex dielectric function $\varepsilon_j=(\varepsilon_1,\varepsilon_2)$ and its effective thickness d_j, and the system's $\Psi(\lambda)$ and $\Delta(\lambda)$ spectra are calculated and compared with the experimental data until the best agreement between simulation and experiment is found by varying the appropriate layer

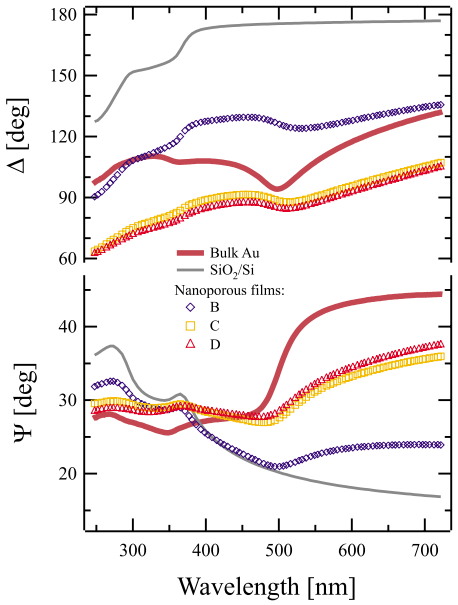

FIG. 3. (Color online) Experimental $\Delta(\lambda)$ and $\Psi(\lambda)$ curves measured for cluster-assembled Au films. Data for samples B, C, and D are reported as the blue, orange, and red symbols, respectively. Clean-substrate (gray lines) and bulk gold (fuchsia lines) ellipsometric spectra are reported for reference.

parameters. Simulations and optical fitting were performed with the aid of the WVASE32 program, supplied by the manufacturer. Measurements were systematically performed at three angles of incidence (60°, 65°, and 70°) though, for the sake of clarity, only the data at 65° will be shown here.

In Fig. 3 we report the $\Psi(\lambda)$ and $\Delta(\lambda)$ spectra measured at 65° of incidence for samples B, C, and D (blue, orange, and red symbols, respectively), approximately 4 days after their fabrication in the SCBD setup. Along with such spectra, reference $\Psi(\lambda)$ and $\Delta(\lambda)$ spectra measured for a typical Si substrate in its as-prepared state, and for a freshly flame-annealed, optically thick (200 nm) Au film deposited on a glass slide coated with a Cr primer (Arrandee) are reported, as the gray and fuchsia lines, respectively. The SiO_2/Si spectra are easily recognizable by their two characteristic features in the UV region, corresponding to the dominant Si absorption peaks. The spectra recorded for sample B accordingly still bear a strong resemblance with the one of the substrate, and exhibit only an overall fading of the Si-related structures in the UV, accompanied by the appearance of Au-related spectral features in the visible part of the spectrum. Increasing the Au film thickness further, the experimental spectra lose any similarities with the initial substrate data, while at the same time not quite approaching the reference Au spectra, even for the thickest film under scrutiny.

At this stage, extracting information about the morphological and electronic properties of the films is possible either by converting the $\Psi(\lambda)$ and $\Delta(\lambda)$ spectra into so-called pseudodielectric functions or by thoroughly modeling the film structure in terms of appropriate layer stacks and corresponding dielectric functions. Whereas the first route was employed in a number of studies,[25,26] it mostly yields qualitative insights only on the actual film properties. The latter,

though harder to implement, yields instead precious quantitative information on the detailed structure of the nanogranular films, and will be the approach of our choice.

III. MODELING SE SPECTRA

A. Au dielectric function

Modeling the optical response of the cluster-assembled films requires taking into account a few basic characteristics, namely, their intrinsically granular nature, their (likely thickness-dependent) porous structure on the nanometer scale and the presence of a marked surface roughness.

For this aim, we will not discuss here the case of isolated clusters (sample A) or the transition between isolated clusters and continuous films,[27,28] but rather focus on the case of thicker films, for which the clusters have aggregated in thicker, three-dimensional structures. For the purpose of this study, the main use of submonolayer samples was that of providing independent information on the size distribution of clusters produced by the SCBD source. At the extremely low coverage needed to reliably measure the cluster size by AFM measurements, the influence of the Au clusters on the bare-substrate response is so small to become noticeable only upon observing the difference between the spectra of sample A and the substrate.[5] Even then, no clear signature of a well-defined surface-plasmon resonance peak[29,30] was observed. This we ascribed to both the poor Au signal at this coverage and to the broadening of the plasmon peak arising from both the size distribution of the Au clusters[7] and from the effects of interaction with the substrate.[31] We point out that detailed treatments of the optical properties of isolated Au particles and structures on various surfaces can be found in a number of publications.[7,32,33]

The granular structure of the films can be modeled by correcting the bulk-Au dielectric constants ε_{bulk} by the introduction of a size-dependent extra contribution $\Delta\varepsilon$ related to enhanced electron scattering in correspondence of cluster boundaries.[6,7,34] Thus, the dielectric constant of the granular medium ε_{ng} will be written as $\varepsilon_{ng}=\varepsilon_{bulk}+\Delta\varepsilon$, where $\Delta\varepsilon$ reads

$$\Delta\varepsilon = \frac{\omega_p^2}{\omega}\left[\frac{1}{\omega + i\Gamma_{bulk}} - \frac{1}{\omega + i\Gamma(R)}\right]. \quad (2)$$

Here ω_p is the plasma frequency and $\Gamma(R)=\Gamma_{bulk}+Av_F/R$, where v_F is the Fermi velocity, Γ_{bulk} is the scattering rate of bulk gold, A is an empirical parameter whose value is typically close to unity,[7,9,29,34,35] and R is the radius of the grain. We assumed bulk values for $v_F=1.4\times10^6$ m/s, $\omega_p=8.8$ eV, and $\Gamma_{bulk}=3.3\times10^{13}$ s^{-1}.[7]

The reference optical constants of bulk gold ε_{bulk} were determined by inversion of the corresponding SE spectra reported in Fig. 3, yielding values in good agreement with benchmark results for this system.[5,7,35] The experimental value for the real and complex part of ε_{bulk} are reported in the top panel of Fig. 4 as the orange and red symbols, respectively. The optical constant ε_{bulk} was then expressed in analytical form, in the form suggested by Etchegoin *et al.*,[36] as the sum of a free-electronlike Drude contribution and of two interband transitions whose defining parameters were adjusted to provide the best fit to the experimental ε_{bulk}. The two interband transitions were located at a wavelength $\lambda=461$ nm and $\lambda=335$ nm, respectively, whereas the plasma wavelength $\lambda_p=2\pi c/\omega_p$ was $\lambda_p=136$ nm, in good agreement with the analysis of Ref. 36. The best-fit curves to ε_{bulk} under this approximation are shown as the solid black lines in the top part of Fig. 4.

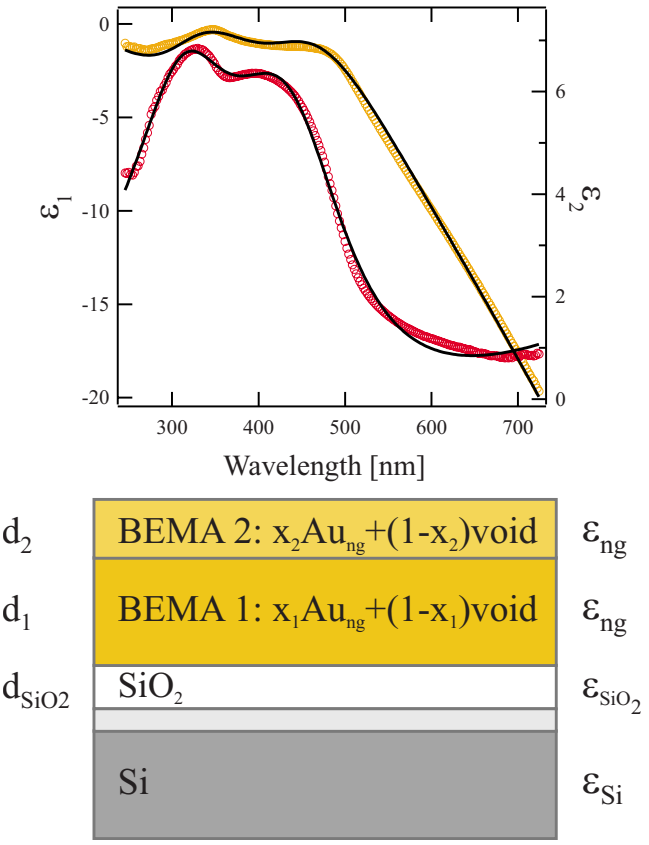

FIG. 4. (Color online) Top panel: real and imaginary part of the bulk-Au dielectric constants extracted from the $\Psi(\lambda)$ and $\Delta(\lambda)$ spectra reported in Fig. 3 (orange and red symbols, respectively). Solid black lines: best fit of the Au dielectric constants, according to the analytical model of Ref. 36. Bottom panel: scheme of the layer stack model employed for fitting the optical response of the cluster-assembled Au films.

As far as the porosity is concerned, we treat the medium with the Bruggeman effective-medium approximation (BEMA).[37] In doing so, some care must be taken, since BEMA approaches fail to correctly reproduce the physical properties of the percolated mixture, like its dielectric constant, in proximity of the percolation threshold.[27,38,39] While we cannot reliably *a priori* assess the proximity of our system to the percolation threshold, we can judge the effectiveness of the BEMA approximation based on its capability of reproducing the experimental spectra. Finally, the thickness dependence of any of the various characteristics of the cluster-assembled systems are conventionally modeled introducing suitable gradings of the film properties (porosity, cluster dimensions, etc.) along the direction normal to the surface.

B. Layer model and fit

The layer model that we adopted for the cluster-assembled Au films, according to the above discussion, is sketched in the bottom part of Fig. 4. The substrate is modeled as an infinitely thick Si layer, topped by a thin SiO_2 film, with a transition layer inserted between the two to allow for possible interdiffusion or inhomogeneity of the Si/SiO_2 interface modeled as a BEMA layer with 50% Si and 50% SiO_2 composition.[21] Tabulated values for the optical constants of Si and SiO_2 have been employed.[40,41] The substrate parameters (thickness of the silicon oxide and of the intermixing layer) were initially optimized by fitting them against the bare-substrate spectra, and subsequently held fixed throughout the fitting procedure of the Au film data. The nanoporous Au film is schematized as a stack of two BEMA layers each consisting of a variable fraction of "granular" gold (with dielectric function ε_{ng}) and voids ($\varepsilon=1$). The BEMA1 layer represents the film fraction in direct contact with the substrate, whereas we label BEMA2 the layer in contact with the ambient. The thickness and the void fraction of the BEMA1 and BEMA2 layers are left free to vary completely independent of each other, whereas the dielectric function ε_{ng} is set to be common to both the BEMA1 and BEMA2 layers, based on the observation that both are formed by the stacking and aggregation of the same precursor clusters.

In the Au films, the parameters left free for optimization were the thickness of each BEMA layer, its void fraction and the finite-size correction $\Delta\varepsilon$ to the bulk-Au dielectric constant. The interband contribution to ε_{ng} was assumed constant and fixed at the bulk value, thereby neglecting any band distortion effect, and the depolarization factor L within each BEMA layer was fixed at $L=1/3$ (spherical inclusions). A number of fitting procedures was performed starting from different sets of initial conditions to ensure the reproducibility of the results. An uncertainty on the order of $\pm 5\%$ on the porosity and of ± 2 nm on the thickness for the Au BEMA layers was estimated.

The best-fit $\Delta(\lambda)$ and $\Psi(\lambda)$ simulated spectra are reported in Fig. 5 on top of the experimental data already shown in Fig. 3. For each sample, the pertinent morphological parameters corresponding to the best-fit spectra are reported in the left part of Fig. 6; the best-fit imaginary part of the granular gold dielectric function ε_{ng} are reported for each sample in the right panels of the figure.

IV. DISCUSSION

In Fig. 5 we notice very good agreement between data and simulations, the only significant discrepancies between the two sets of curves being found for the C and D samples in the UV regions. We are accordingly confident of the ability of our model to capture the essential characteristics of the nanoporous materials, thereby also justifying the description of the effective dielectric properties of the mixture in terms of the BEMA approach. The best-fit procedures yield different thickness of the nanoporous Au layer, ranging form little more than 10 nm for film B to almost 60 nm for sample D. However, despite this relatively large film thickness range,

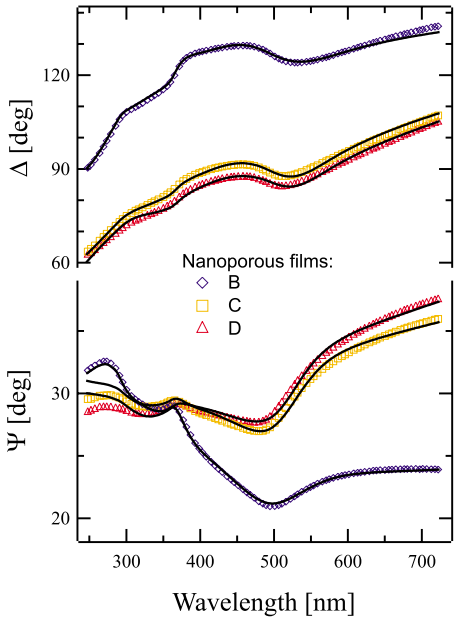

FIG. 5. (Color online) Experimental and simulated $\Delta(\lambda)$ and $\Psi(\lambda)$ curves for the cluster-assembled Au films. Experimental data for substrate and samples B, C, and D are reported as the blue, orange, and red symbols, respectively. Best-fit simulated $\Delta(\lambda)$ and $\Psi(\lambda)$ curves, according to the model described in the text, are reported as the solid black lines and superimposed to the corresponding experimental data.

many similarities appear in the morphological characteristics of the samples. The BEMA1 layers, i.e., the porous Au layer in direct contact with the substrate, exhibit a fairly similar porosity ranging between 22% and 35% over the various samples, whereas the BEMA2 layer is consistently more porous for all the samples, with void percentages ranging between 69% and 83%. This suggests that the "inner" film layers are characterized by a metallic behavior whereas in the BEMA2 layer some degree of spatial confinement might occur. For each sample, we also notice that the thickness of the BEMA2 layer exhibits a very clear linear scaling with the corresponding BEMA1 thickness, and we stress that the best-fit procedure yields dielectric functions ε_{ng} for the granular Au which are extremely similar over the three different samples, showing markedly larger values at the near infrared end of the spectrum with respect to the reference Au dielectric function ε_{bulk}. The information extracted from the fitting therefore provides interesting insights on both the morphological and the electronic properties of the cluster-assembled films that are worth discussing further.

In this respect, the first point we address concerns the degree of porosity obtained for the two effective-medium layers. For the BEMA1 layer, we obtain relative densities of the cluster film with respect to a corresponding bulk system roughly between 0.65 and 0.8. These values are in very good agreement with molecular-dynamics simulations performed for cluster-assembled Au films employing realistic cluster-size distributions[42] that predict 0.6 relative density for 0.25 eV/atom deposition energy and 0.95 for the 1.25 eV/atom case (note that these deposition energies are comparable to ours). In the BEMA2 layer, instead, much lower relative den-

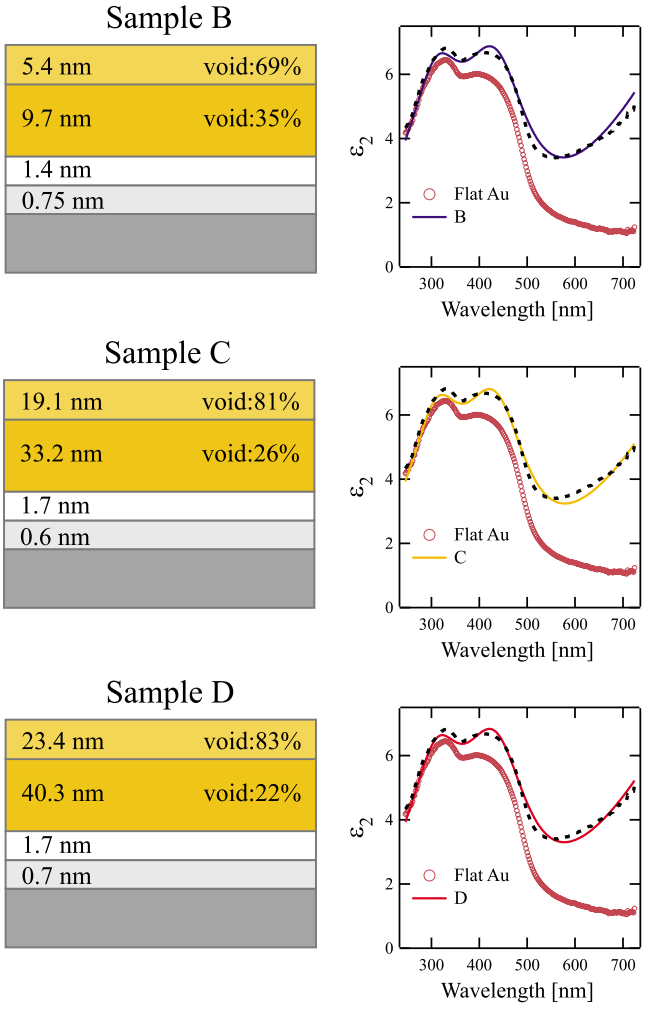

FIG. 6. (Color online) Left: layer models corresponding to the best-fit curves for samples B, C, and D. The best-fit value for the layer thickness is indicated, along with the void fraction, where applicable. Right: imaginary part of the dielectric function ε_{ng} corresponding to the best-fit simulations for samples B, C, and D (blue, orange, and red lines, respectively). The dielectric function of bulk gold is reported for reference as the open symbols. The dashed black line is the calculated value for the dielectric function of a gold cluster with radius $R \approx 4$ nm.

sities roughly within the 0.2–0.3 range are extracted via the optical modeling. The BEMA2 layer can be accordingly viewed as an effective surface roughness layer for the porous films,[42] in strict analogy with the optical modeling of surface roughness adopted in bulk samples.[34] According to our model, the BEMA2 thickness scales linearly with respect to the BEMA1 thickness, in substantial agreement with previous experimental observations and with independent calculations carried out for cluster-assembled films.[42,43] Overall, the good matching between the outcome of the optical model and the independent information available from the literature confirms the quantitative reliability of the information derived from our analysis, and supports us in discussing the nanoporous Au effective dielectric constants, reported in the right panels of Fig. 6. There, the best-fit wavelength dependences of ε_{ng} for samples B, C, and D are reported as the blue, orange, and red lines, respectively. According to Eq. (2), the marked increase in ε_{ng} at long wavelength with respect to ε_{bulk} is a clear fingerprint of the corresponding reduction of the electron mean-free path in our samples. From the ε_{ng} curves, the mean effective radius R of the Au grains within the porous film can be deduced applying Eq. (2), provided a reliable value of the parameter A is available. In the literature, values of A with some spread between roughly 1 and 2 have been reported.[7,9,29] Assuming a value of $A=4/3$, as employed in Ref. 7 for colloidal suspensions, we obtain a mean diameter of the grains $d \approx 9$ nm while employing $A=1$, as suggested by Aspnes[34] for morphologically continuous Au films, yields a slightly lower mean diameter $d \approx 6.75$ nm. We can safely assume that the correct value lies in between these extrema with a propension for the "continuous-film" value of $A=1$. The imaginary part of the dielectric function that matches best the results of the fits, calculated under these assumptions is reported as the dashed black line in the panels on the right side of Fig. 6.

The mean cluster size deduced by ellipsometry can be now meaningfully compared with the one deduced on the basis of the AFM characterization of submonolayer samples, allowing to deduce the degree of mutual cluster coalescence when assembled in the three-dimensional porous film structure. However, a bit of care is required in doing this, since it can be expected that each precursor cluster will contribute to the overall optical response of the material not according to its relative abundance, but rather to the relative volume it occupies within the film. Hence, the relevant cluster-size distribution to be compared with the results of the optical analysis is not the basic cluster-size distribution, but rather the volume fraction distribution, reported in Fig. 2 as the orange solid bars, that effectively "weighs" each cluster's contribution according to its volume. This distribution, that peaks at $d \approx (6.5 \pm 2)$ nm, provides a value of the "effective" mean cluster size which is compatible with the one deduced via the optical modeling.

While pointing out the remarkable fact of achieving such a similarity between two measurements obtained by two very different methods, we suggest that this finding is a strong indication that the clusters mostly retain their crystallographic individuality when assembled in the film. Thus, despite giving rise in the BEMA1 case to a typically metallic behavior, the clusters apparently do not achieve epitaxial alignment upon getting in contact with one another. This result closely agrees with existing simulations predicting the tendency of randomly deposited metal clusters with deposition energy comparable to ours to maintain their own crystallographic alignment upon assembly in "thick" films, with the consequent formation of various crystal defects at cluster boundaries.[44–46] From the point of view of the optical response, the contact of the clusters upon their stacking gives rise to long-range electrical conduction paths in the film that apparently suppress any spectral feature derived from localized plasmon resonances. However, the absence of mutual coherent epitaxial alignment between the clusters still causes an increase in the electron-scattering rate at the cluster contact points, thereby provoking the extra Drude-type absorption, that is, clearly visible in the low-energy side of the best-fit dielectric functions ε_{ng} even in absence of spatial

confinement. Interestingly, our model also suggests a substantial independence of the effective mean grain size upon the film thickness. This indicates that the energy deposited in the film by the impinging clusters during deposition does not induce major film annealing or a rearrangement of the clusters sufficient to substantially reduce the amount of crystallographic defects relevant for the free-carrier scattering as the film thickness is increased. What we cannot instead exclude from our data is the fact that the smallest clusters (diameter $\lesssim 2-3$ nm), that are relatively abundant in the size distribution, might achieve some degree of epitaxial alignment upon landing onto larger particles, as the theory indeed suggests.[42] In this case, the net effect would be a depletion of the low-size tail of the precursor cluster distribution of Fig. 2 in favor of larger clusters that would effectively push the mean cluster size in the films to a value higher than the original distribution. Under this assumption, the agreement between the ellipsometric and the AFM analysis would be even stronger.

V. CONCLUSION

In conclusion, we have investigated the morphological properties of thin nanoporous Au films deposited by soft cluster assembly, i.e., in the absence of surfactants, onto a silicon surface. We have developed a simple model to characterize the nanoporous films based on the analysis of their optical response, explicitly including both finite-size effects due to the granular nature of the material, and the material porosity. The analysis of the optical measurements performed according to such model allowed to extract the morphological parameters defining the film properties, such as its thickness, roughness, degree of porosity, and mean effective size of the constituents clusters. These data were compared with the results of theoretical simulations on analogous systems available in the literature, and with a microscopic characterization of the precursor clusters performed by AFM, yielding a remarkably good agreement in all these aspects. In particular, the effective size of the clusters deduced by spectroellipsometry nicely matched the data extracted by AFM analysis, thereby suggesting the occurrence of limited cluster coalescence in the film during the deposition. Within this framework, the analysis of the optical response of the cluster-assembled films appears as a fast probe of sample properties, such as the degree of epitaxial alignment of the clusters within the film interior that, although extremely precious for understanding the system's behavior, are typically complex to obtain from experiments.

Characterizing material porosity by ellipsometric techniques,[47,48] is nowadays a well-established method, that typically relies on the observation and modeling of adsorption-desorption vapor isotherms from the system under scrutiny. In this respect, our work employs a different physical mechanism for determining the pore characteristics, in which no interaction with the environment is required. Thanks to this, both closed and open pores in the material are observable, and typical pore dimensions reaching the nanometric domain can be accounted for, with no need of modeling the vapor properties inside the pores. We accordingly believe that our work gives a further strong contribution in promoting spectroscopic ellipsometry as a powerful and noninvasive characterization tool for nanoporous structures with possibly relevant fallouts in highlighting molecule-surface interactions in confined geometries.

ACKNOWLEDGMENTS

The authors acknowledge A. Podestà (Università degli Studi di Milano, Dipartimento di Fisica) for performing part of the AFM measurements. F.B. acknowledges the CNR-CNISM convention for financial support. Financial support from the Università di Genova (PRA 2008) and the Fondazione Carige is acknowledged.

*bisio@fisica.unige.it

[1] J. Erlebacher, M. J. Aziz, A. Karma, N. Dimitov, and K. Sieradski, Nature (London) **410**, 450 (2001).
[2] F. Yu, S. Ahl, A.-M. Caminade, J.-P. Majoral, W. Knoll, and J. Erlebacher, Anal. Chem. **78**, 7346 (2006).
[3] M. D. Malinsky, K. L. Kelly, G. C. Schatz, and R. P. Van Duyne, J. Am. Chem. Soc. **123**, 1471 (2001).
[4] K.-S. Lee and M. A. El-Sayed, J. Phys. Chem. B **110**, 19220 (2006).
[5] M. Prato, R. Moroni, F. Bisio, R. Rolandi, L. Mattera, O. Cavalleri, and M. Canepa, J. Phys. Chem. C **112**, 3899 (2008).
[6] H. Hövel, S. Fritz, A. Hilger, U. Kreibig, and M. Vollmer, Phys. Rev. B **48**, 18178 (1993).
[7] E. S. Kooij, H. Wormeester, E. A. M. Brouwer, E. van Vroonhoven, A. van Silfhout, and B. Poelsema, Langmuir **18**, 4401 (2002).
[8] G. B. Smith, A. I. Maaroof, and A. Gentle, Opt. Commun. **271**, 263 (2007).
[9] V. Amendola and M. Meneghetti, J. Phys. Chem. C **113**, 4277 (2009).
[10] T. Mazza, E. Barborini, I. N. Kholmanov, P. Piseri, G. Bongiorno, S. Vinati, P. Milani, C. Ducati, D. Cattaneo, A. Li Bassi, C. E. Bottani, A. M. Taurino, and P. Siciliano, Appl. Phys. Lett. **87**, 103108 (2005).
[11] R. Carbone, I. Marangi, A. Zanardi, L. Giorgetti, E. Chierici, G. Berlanda, A. Podestà, F. Fiorentini, G. Bongiorno, P. Piseri, P. G. Pelicci, and P. Milani, Biomaterials **27**, 3221 (2006).
[12] A. Perez, P. Melinon, V. Dupuis, P. Jensen, B. Prevel, J. Tuaillon, L. Bardotti, C. Martet, M. Treilleux, M. Broyer, M. Pellarin, J. L. Vaille, B. Palpant, and J. Lerme, J. Phys. D **30**, 709 (1997).
[13] T. Ung, L. M. Liz-Marzan, and P. Mulvaney, J. Phys. Chem. B **105**, 3441 (2001).
[14] E. Barborini, P. Piseri, and P. Milani, J. Phys. D **32**, L105 (1999).
[15] K. Wegner, P. Piseri, H. Vahedi Tafreshi, and P. Milani, J. Phys. D **39**, R439 (2006).

[16] P. Liu, P. J. Ziemann, D. B. Kittelson, and P. H. McMurry, Aerosol Sci. Technol. **22**, 293 (1995).
[17] H. Haberland, Z. Insepov, and M. Moseler, Phys. Rev. B **51**, 11061 (1995).
[18] P. Melinon, G. Fuchs, B. Cabaud, A. Hoareau, P. Jensen, V. Apillard, and M. Treilleux, J. Phys. I **3**, 1585 (1993).
[19] P. Milani, E. Barborini, P. Piseri, C. E. Bottani, and A. Li Bassi, Eur. Phys. J. D **9**, 63 (1999).
[20] E. Barborini, I. N. Kholmanov, A. M. Conti, P. Piseri, S. Vinati, P. Milani, and C. Ducati, Eur. Phys. J. D **24**, 277 (2003).
[21] G. Gonella, O. Cavalleri, I. Emilianov, L. Mattera, M. Canepa, and R. Rolandi, Mater. Sci. Eng., C **22**, 359 (2002).
[22] R. M. A. Azzam and N. M. Bashara, *Ellipsometry and Polarized Light* (Elsevier, Amsterdam, North Holland, 1987).
[23] H. Tompkins and E. Irene, *Handbook of Ellipsometry* (Noyes Data Corporation/Noyes, Park Ridge, NJ, 2005).
[24] J. A. Woollam, C. L. Bungay, L. Yan, D. W. Thompson, and J. N. Hilfiker, Proc. SPIE **4932**, 393 (2002).
[25] M. C. Dixon, T. A. Daniel, M. Hieda, D. M. Smilgies, M. H. W. Chan, and D. L. Allara, Langmuir **23**, 2414 (2007).
[26] A. J. de Vries, E. S. Kooij, H. Wormeester, A. A. Mewe, and B. Poelsema, J. Appl. Phys. **101**, 053703 (2007).
[27] Y. Yagil, P. Gadenne, C. Julien, and G. Deutscher, Phys. Rev. B **46**, 2503 (1992).
[28] T. Brandt, M. Hövel, B. Gompf, and M. Dressel, Phys. Rev. B **78**, 205409 (2008).
[29] U. Kreibig and L. Genzel, Surf. Sci. **156**, 678 (1985).
[30] U. Kreibig and M. Vollmer, *Optical Properties of Metal Clusters* (Springer Verlag, Berlin, 1995).
[31] C. Noguez, J. Phys. Chem. C **111**, 3806 (2007).
[32] I. Doron-Mor, Z. Barkay, N. Filip-Granit, A. Vaskevich, and I. Rubinstein, Chem. Mater. **16**, 3476 (2004).
[33] B. Gompf, J. Beister, T. Brandt, J. Pflaum, and M. Dressel, Opt. Lett. **32**, 1578 (2007).
[34] D. E. Aspnes, E. Kinsbron, and D. D. Bacon, Phys. Rev. B **21**, 3290 (1980).
[35] U. Kreibig, J. Phys. F: Met. Phys. **4**, 999 (1974).
[36] P. G. Etchegoin, E. C. L. Ru, and M. Meyer, J. Chem. Phys. **125**, 164705 (2006).
[37] D. A. G. Bruggeman, Ann. Phys. **24**, 636 (1935).
[38] A. L. Efros and B. I. Shklovskii, Phys. Status Solidi B **76**, 475 (1976).
[39] J. P. Clerc, G. Giraud, J. M. Laugier, and J. M. Luck, Adv. Phys. **39**, 191 (1990).
[40] *Handbook of Optical Constants of Solids*, edited by E. D. Palik (Academic, New York, 1985).
[41] C. M. Herzinger, B. Johs, W. A. McGahan, J. A. Woollam, and W. Paulson, J. Appl. Phys. **83**, 3323 (1998).
[42] L. Bardotti, B. Prével, P. Mélinon, A. Perez, Q. Hou, and M. Hou, Phys. Rev. B **62**, 2835 (2000).
[43] R. Buzio, E. Gnecco, C. Boragno, U. Valbusa, P. Piseri, E. Barborini, and P. Milani, Surf. Sci. **444**, L1 (2000).
[44] Q. Hou, M. Hou, L. Bardotti, B. Prével, P. Mélinon, and A. Perez, Phys. Rev. B **62**, 2825 (2000).
[45] C. Huang, W. T. Nichols, D. T. O'Brien, M. F. Becker, D. Kovar, and J. W. Keto, J. Appl. Phys. **101**, 064902 (2007).
[46] K. Meinander and K. Nordlund, Phys. Rev. B **79**, 045411 (2009).
[47] M. R. Baklanov, K. P. Mogilnikov, V. G. Polovinkin, and F. N. Dultsev, J. Vac. Sci. Technol. B **18**, 1385 (2000).
[48] C. Boissiere, D. Grosso, S. Lepoutre, L. Nicole, A. Brunet Bruneau, and C. Sanchez, Langmuir **21**, 12362 (2005).